Complex Phasor Modeling and Control of Modular Multilevel Inverters

Justin Reed, Giri Venkataramanan
Dept. of Electrical and Computer Engineering
University of Wisconsin-Madison
Madison, WI 53706, USA
jkreed@ieee.org, giri@engr.wisc.edu

Francisco Martínez
Department of Electrical Engineering
ETSI Industriales – Technical University of Madrid
Madrid, Spain
fcmartinezgarcia@yahoo.es

***Abstract*— Modular multilevel power converters in a 'bridge of bridge' configuration have been introduced recently for realizing ac-dc, dc-ac and ac-ac power conversion functions with voltage step-up and step-down capability, bidirectional power flow and transformerless operation. While different modulation and control approaches have been introduced in an ad-hoc manner in the introductory literature, definitive models that may be used to characterize the steady state and dynamic performance are just beginning to be uncovered. It is the objective of this paper to introduce a canonical phasor or complex vector model to represent the ac variables along with the dc variables that are unique to this family of converters. The model is used to develop a suitable control approach using established techniques. The complex vector model is represented in the synchronously rotating *dq* reference frame, and illustrated using an application of a dc-ac step-up inverter for residential photovoltaic applications.**

I. INTRODUCTION

While commercially established topologies of multilevel converters may be of dc stack type, flying capacitor type, or cascaded H-bridge type, more recently, the modular multilevel converter (M2C) topology that may be viewed as a 'bridge of bridge' converter (BoBC) topology has been introduced as a versatile approach for realizing bidirectional dc-ac, ac-dc, or ac-ac power conversion with voltage step up or down without the use of transformers [1] in a wide range of applications. Much of the introductory literature that focused on establishing the topological capability has demonstrated its operational capability using ad-hoc approaches to modulation and control [2, 3]. More recently an analytical model for the converter based on averaged modeling of the switching elements has been introduced that may be used for developing more definitive approaches towards modulation and control [1]. The dynamic variables of the converter feature substantial power frequency quantities occurring in the mixed mode – i.e. dc and ac superimposed, etc., posing strong coupling relationships. A complex phasor or dq model, wherein the ac quantities are represented in a synchronously rotating reference frame, are presented in this paper and allow the quantities to be decoupled while uncovering power transfer mechanisms succinctly. Such a model allows the application of canonical approaches to ac power converter control to the emerging family of power converters.

A photovoltaic (PV) power converter that is operated in a power control mode is used as an illustrative example for presenting the dq equivalent circuit model for the converter and developing a suitable controller. In order to boost the dc voltage to the requisite ac grid voltage, conventional PV power converters typically use either a line frequency transformer or a separate dc-dc boosting stage [4, 5], both of which require significant magnetic components. The BoBC provides the same conversion capability without a transformer and in only one conversion stage, reducing weight and bulk.

The BoBC is introduced in Section II, which provides a general view of how the BoBC is constructed including its 'building blocks,' followed by the specific single-phase dc-ac BoBC topology used in this paper. Sections III and IV present the converter dynamic scalar and phasor models, respectively. The overall control scheme is discussed in detail in Section V, followed by validation of the modeling and controller development in Section VI.

II. BOBC TOPOLOGY

A. General BoBC Topology

The generalized BoBC is a bridge arrangement of small bridge 'building blocks.' These building blocks, hereby referred to as capacitive storage embedded bridges (CSEBs or *bridges* for short), contain a capacitive energy store, a bridge arrangement of switches, and a small amount of series inductance. An arbitrary number of bridges placed in series and/or parallel form a *branch*, which behaves as a controlled current source wherein the current is controlled by modulating the bridge voltages according to the instantaneous terminal voltages. An entire dc-ac converter is then constructed from $2n_{br}$ branches in a bridge configuration, where n_{br} represents the number of bridges connected to a single dc terminal. Each branch current contains an appropriate combination of dc and

978-1-4577-0541-0/11/$26.00 ©2011 IEEE

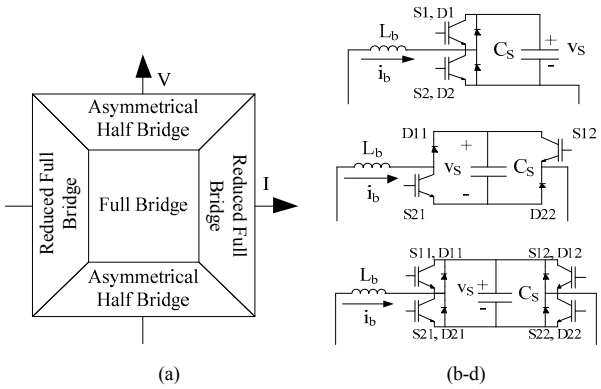

Fig. 1. CSEB types using IGBTs: (a) terminal V-I characteristics, (b) asymmetrical half bridge, (c) reduced full bridge, and (d) full bridge. Switch and diode numbering are shown for clarity.

ac components such that the ac components add at the ac terminals and cancel at the dc terminals, and vice-versa.

Within the BoBC, three types of CSEBs may be used: the asymmetrical half bridge, the reduced full bridge, and the full bridge, all shown in Fig. 1. Fig. 1a illustrates the operating quadrants of CSEBs, while the corresponding realizations are shown in Figs. 1b-d. Notably, while the full bridge is capable of bidirectional current and bidirectional voltage, the asymmetrical half bridge is capable of only unidirectional (or zero) voltage, while the reduced full bridge is limited to unidirectional current. Each 2-terminal CSEB is incapable of real power sourcing or sinking, aside from a small amount of losses, therefore CSEB power flow must be reactive. As such, all CSEBs must provide at least 2 quadrants of operation in the VI plane, as shown in Fig. 1a.

B. Single Phase DC-AC Converter

A candidate 1 kW residential photovoltaic (PV) step-up converter from 48 V dc to a 3-wire 230 V 60 Hz ac grid connection is shown in Fig. 2a with one grounded dc-side conductor (the mid-point), as mandated by the National Electrical Code (NEC) Section 690.41 [6]. Each branch of the converter comprises n_s=5 series connected reduced full bridge CSEBs. A simplified equivalent circuit of the series connected bridges represented by a single controlled current source is shown in Fig. 2b. By symmetry of the bridge, the entire converter behavior may be modeled in terms of the CSEBs within each branch, such as with the CSEB dynamic scalar model shown in Fig. 2c.

III. CSEB DYNAMIC SCALAR MODELING

A time-domain scalar averaged model for the BoBC was proposed in [1], and as applied to the converter illustrated in Fig. 2 for $1 \le j \le 2$ and $1 \le k \le 3$, may be expressed as

$$n_s L_b \frac{di_{b(j,k)}(t)}{dt} = V_{dc,j} - V_{ac}\cos[\omega_{ac}t - (k-1)\pi] - n_s d_{b(j,k)}(t) v_{S(j,k)}(t) \quad (1)$$

$$C_{S(j,k)} \frac{dV_{S(j,k)}}{dt} = d_{b(j,k)}(t) i_{b(j,k)}(t) \quad (2)$$

With an appropriately sized bridge energy storage capacitor C_S leading to small enough ac ripple voltage component on V_S, the steady state circuit solutions for (1) and (2) may be shown to be

$$V_{S(j,k)}(t) \approx V_{S,dc} \quad (3)$$

$$i_{b(j,k)}(t) = \frac{I_{dc}}{3} - (-1)^k \frac{I_{ac}}{2}\cos[\omega_{ac}t - (k-1)\pi - \varphi_{ac}], \quad (4)$$

where $V_{S,dc}$ is a constant. The fidelity of this averaged dynamic representation has been demonstrated using laboratory experiments illustrated in Fig. 3 [1]. For convenience, the variable naming nomenclature used in the scalar and phasor modeling of this paper is provided in the appendix.

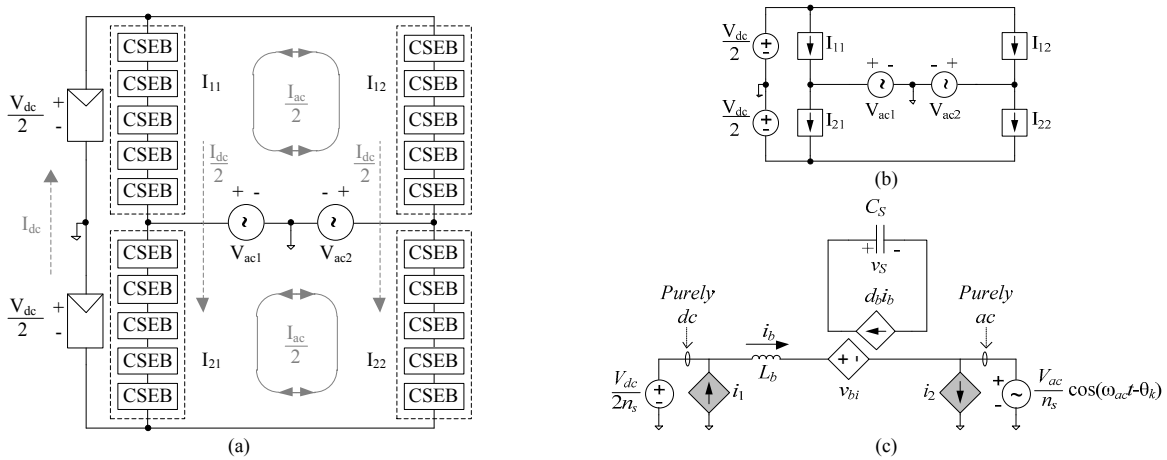

Fig. 2. (a) Architecture of a 1-phase BoBC dc-ac step-up converter with n_s=5, (b) simplified equivalent circuit, and (c) averaged scalar model of one CSEB. The current sources i_1 and i_2 represent the nulling component currents at each external terminal to ensure pure dc components from V_{dc} and pure ac components at V_{ac}.

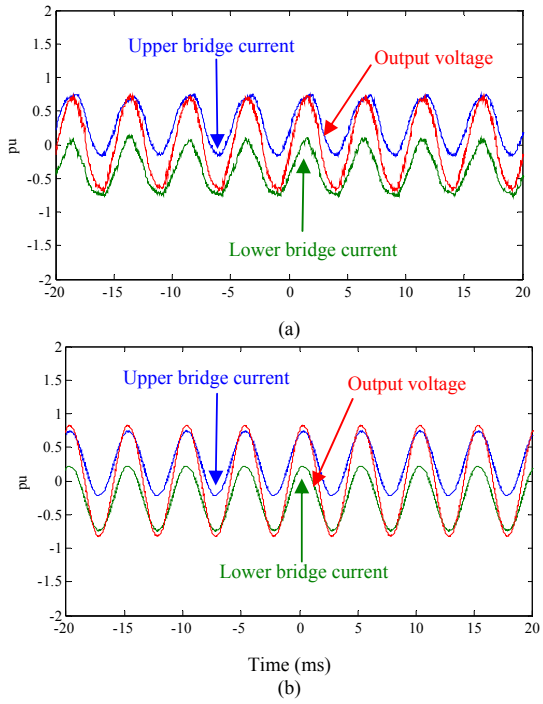

Fig. 3. Experimental and simulated waveforms using averaged scalar model for a laboratory-scale dc-1φ/200-Hz-ac BoBC modular multilevel converter with 2 CSEBs switching at 20 kHz [1].

IV. CSEB Dynamic Phasor Model

Since the branch currents and voltages include dc and ac components, they may be represented by their appropriate phasor representations in the synchronous reference frame. Adopting the dq model in the complex plane where the d-axis corresponds with the positive real axis, the q-axis corresponds with the positive imaginary axis, and the terminal ac voltage phasor V_{ac} is purely real, the following time-domain identities may be established for branch (1,1) and readily extended for all branches:

$$i_b(t) = I_{b,dc} + \mathrm{Re}\left\{\underline{I}_{b,ac} e^{j\omega_{ac}t}\right\} \tag{5}$$

$$d_b(t) = D_{b,dc} + \mathrm{Re}\left\{\underline{D}_{b,ac} e^{j\omega_{ac}t}\right\} \tag{6}$$

$$V_S(t) = V_{S,dc}\,, \tag{7}$$

where an underline indicates a complex variable. With such complex representations for the time domain scalar variables, the dynamic phasor relationships for the capacitor and inductor are

$$C_S \frac{dV_S}{dt} = \left(I_{b,dc} + \underline{I}_{b,ac} e^{j\omega_{ac}t}\right)\overline{\left(D_{b,dc} + \underline{D}_{b,ac} e^{j\omega_{ac}t}\right)} \tag{8}$$

$$\begin{aligned} n_s L_b \frac{d}{dt}\left[I_{b,dc} + \underline{I}_{b,ac} e^{j\omega_{ac}t}\right] = {} & \frac{V_{dc}}{2} - n_s D_{b,dc} V_{S,dc} \\ & - n_s \underline{D}_{b,ac} V_{S,dc} e^{j\omega_{ac}t} \\ & - V_{ac} e^{j\omega_{ac}t} \end{aligned} \tag{9}$$

where the over-bar indicates a complex conjugate, due to both quantities being phasors. Neglecting higher order terms, the dc, fundamental ac real/direct and fundamental ac imaginary/quadrature components may then be extracted from each equation into (10-13). This dynamic phasor model may also be represented in circuit diagram form, such as in Fig. 4, or in block diagram form as shown in Fig. 5.

$$\begin{aligned} C_S \frac{dV_S}{dt} = {} & D_{b,dc} I_{b,dc} + \tfrac{1}{2} D_{b,ac,d} I_{b,ac,d} \\ & + \tfrac{1}{2} D_{b,ac,q} I_{b,ac,q} \end{aligned} \tag{10}$$

$$n_s L_b \frac{dI_{b,dc}}{dt} = \frac{V_{dc}}{2} - n_s D_{b,dc} V_{S,dc} \tag{11}$$

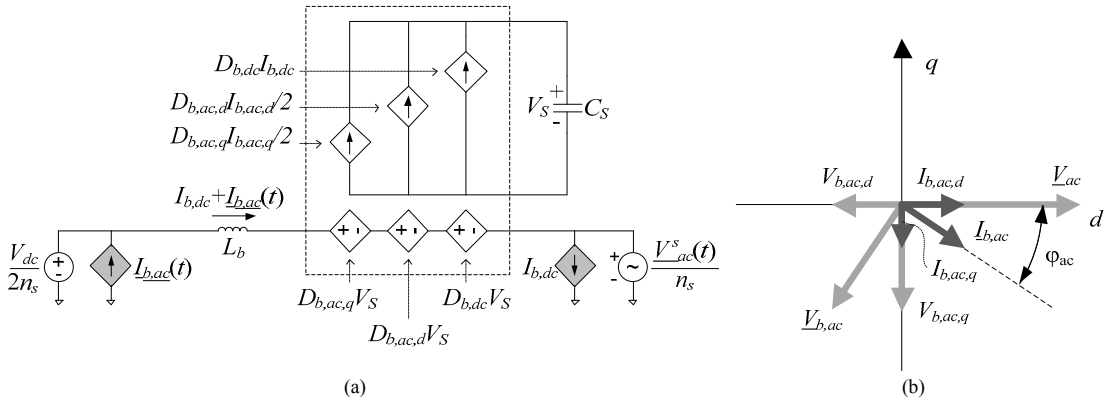

Fig. 4. (a) Phasor model of single CSEB within BoBC, (b) phasor diagram of circuit quantities. The sources $I_{B,ac}(t)$ and $I_{B,dc}$ represent the branch ac and dc currents, respectively, which flow as a result of the multiple branch connections at each converter terminal.

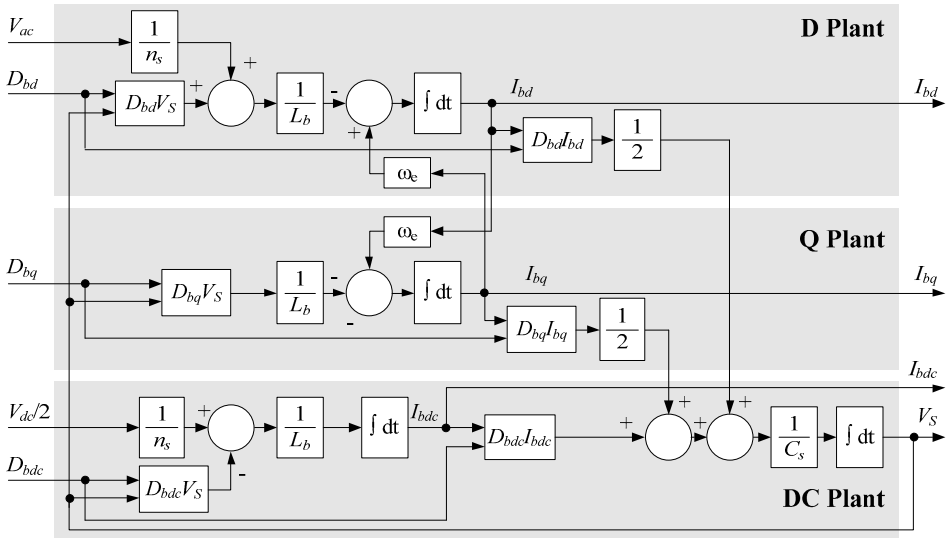

Fig. 5. CSEB plant phasor model block diagram.

$$n_s L_b \frac{dI_{b,ac,d}}{dt} = \omega_{ac} L_b I_{b,ac,q} - n_s D_{b,ac,d} V_{S,dc} - V_{ac} \quad (12)$$

$$n_s L_b \frac{dI_{b,ac,q}}{dt} = -\omega_{ac} L_b I_{b,ac,d} - n_s D_{b,ac,q} V_{S,dc} \quad (13)$$

Several key features of the dynamic phasor model are evident. First, in steady-state operation the dc and real ac power of each bridge must be balanced, which is represented in the capacitor current equation (10) and must equal zero on average. From a purely power balancing perspective, when the input and output power of a system is unbalanced, the system must account for the difference. In this case, should an imbalance occur, the energy store absorbs the power difference and the capacitor voltage changes accordingly. Due to the representation of phasor quantities by their sinusoidal peak values, the d and q axis current components and duty ratio products in (10) are scaled by ½ to their rms values in order to balance with the dc components.

Second, the d and q axis cross-coupling current terms in (12-13) are not only evident but also typical of phasor representations of ac variables in dynamic form [7]. In the absence of the cross-coupled terms, (11-13) describe three separate and easily controlled dynamic systems. Therefore, a proper control scheme can overcome this non-ideal cross-coupling behavior by properly decoupling the current components from each other, as well as maintaining control over the capacitor voltage by modulating the quantities in (10). Such a control scheme is discussed next.

V. Photovoltaic Converter Control

The proposed complex vector model consisting of dc and direct and quadrature ac components of bridge variables has been applied to the control of the residential solar electric inverter system illustrated in Fig. 2a. A high level block diagram of the hierarchical controller's top level is shown in Fig. 7. A hierarchical structure is chosen to leverage the core advantages of both centralized and distributed control techniques.

While a centralized controller is advantageous for terminal current regulation, at the same time its biggest weakness is the number of voltage sensing and gate signals required; for large numbers of CSEBs the number of I/O ports can become

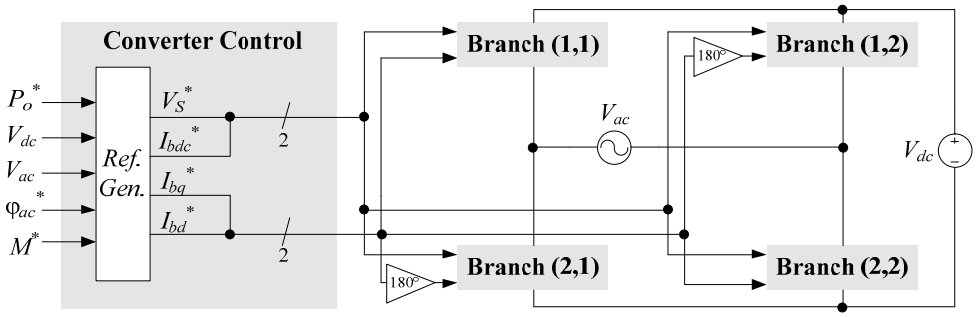

Fig. 6. Converter controller, illustrating reference generator and communications to branch controllers.

prohibitive. A distributed controller structure, while greatly reducing the I/O port requirement by localizing the voltage sensing and gate signals to each CSEB, is less effective for enforcing collective control over all CSEBs in order to regulate the terminal currents. Such a control structure would not be straightforward to design such that individual CSEB current control loops did not interfere with each other, particularly those located in the same branch.

A hierarchical (or hybrid) structure leverages the strengths of both methods. The controller consists of a centralized 'Ref. Gen.' (reference generator) which provides appropriate branch current command signals for each of the branch controllers based on the desired amount of power transfer. These branch currents then transfer power between the source and load. Each of the branch controllers regulates the branch currents through a proportional feedback loop 'P' operating in the dq-dc synchronous reference frame as shown in Fig. 7a. The branch controller provides a so-called *internal* bridge voltage command for each of the bridge controllers, which represents the voltage to be applied by each bridge to yield the desired di/dt for current regulation, as illustrated in Fig. 7b.

The bridges, each with its own controller, function as voltage sources between source, load, and inductance. As shown in the various averaged models presented, the bridge duty ratio affects both the inductor current and the capacitor voltage. Therefore, each bridge controller incorporates a locally operating 'PI' regulator that maintains the energy storage capacitor voltage at the desired value by augmenting the internal bridge voltage commands, and thus its duty ratios, accordingly as illustrated in Fig. 7b. Together, the three levels of control provide an effective method of achieving all voltage and current regulation requirements while minimizing necessary communication between controllers and between CSEBs.

A. Controller Implementation

Based on the commanded power throughput P_o^*, measured dc and ac voltages V_{dc} and V_{ac}, desired power factor φ_{ac}^*, and commanded modulation index M^*, the reference generator in Fig. 6 produces bridge energy storage voltage command V_S^*, and branch current commands I_{bdc}^*, I_{bd}^* and I_{bq}^* according to:

$$V_S^* = \frac{1}{M^*}\left(\frac{V_{dc}}{2} + V_{ac}\right) \tag{14}$$

$$I_{bdc}^* = \frac{P_o^*}{2V_{dc}} \tag{15}$$

$$I_{bd}^* = \frac{P_o^*}{2V_{ac}} \tag{16}$$

$$I_{bq}^* = \frac{P_o^* \tan\left(\varphi_{ac}^*\right)}{2V_{ac}} \tag{17}$$

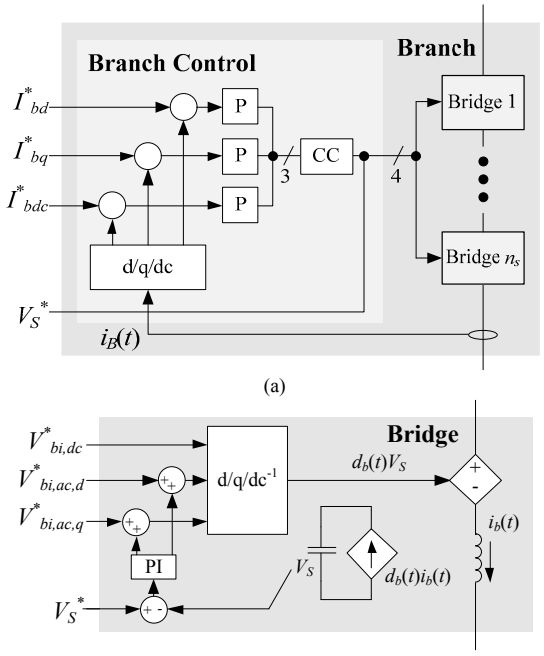

Fig. 7. Structures of (a) branch controller and (b) bridge controller, where the d/q/dc and d/q/dc^{-1} blocks represent transformations between instantaneous and phasor domain variables.

Each branch controller, shown in Fig. 6 and Fig. 7a, controls the d, q, and dc branch current components using proportional gains K_{pId}, K_{pIq}, and K_{pIdc}, respectively. The measured current values are converted from the actual scalar measurement into d, q and dc components with a d/q/dc transformation synchronized with the grid voltage. The outputs of the branch controller are the internal bridge voltage commands V_{ibd}^*, V_{ibq}* and V_{ibdc}*. Cross-coupling of I_{bd} and I_{bq} is removed in the 'CC' block, yielding

$$V_{ibd}^* = -\frac{V_{ac}}{n_s} - \frac{K_{pId}}{n_s}\left(I_{bd}^* - I_{bd}\right) + \omega_{ac} L_b I_{bq} \tag{18}$$

$$V_{ibq}^* = -\frac{K_{pIq}}{n_s}\left(I_{bq}^* - I_{bq}\right) - \omega_{ac} L_b I_{bd} \tag{19}$$

$$V_{ibdc}^* = \frac{V_{dc}}{2n_s} - \frac{K_{pIdc}}{n_s}\left(I_{bdc}^* - I_{bdc}\right). \tag{20}$$

All the details of the branch current regulators are represented in the block diagram of Fig. 8.

As shown in Fig. 7a, the energy storage capacitor voltage command V_S^* is fed through directly to the bridge controllers, which are illustrated in Fig. 7b. Proportional and integral gains K_{iVs_ac} and K_{pVs_ac} provide the gains for voltage regulation. This is shown in more detail in Fig. 9, which includes the bridge plant as well as the voltage regulator. The integral voltage error term is denoted V_{ib_err}.

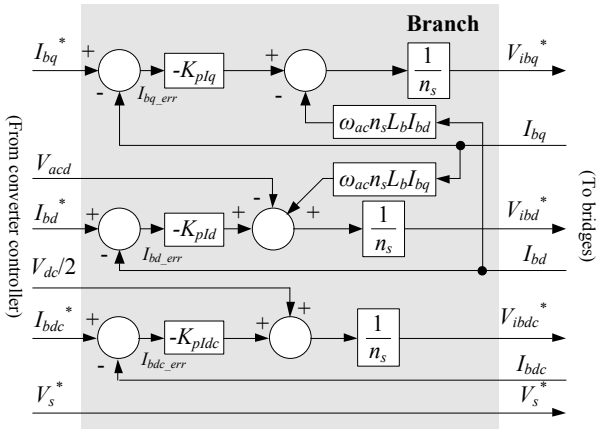

Fig. 8. Branch controller block diagram, including cross-coupling compensation and current regulator proportional gains.

The complete set of state equations for the system including all of the controllers is:

$$\begin{aligned}\frac{dV_S}{dt} = \frac{1}{V_S C_S}\Bigg[&\frac{-K_{pIq} I_{bq}}{2n_s}\left(I_{bq}^* - I_{bq}\right)..\\ &-\frac{I_{bd}}{2n_s}\left(V_{ac} + K_{pId}\left(I_{bd}^* - I_{bd}\right)\right)..\\ &+\frac{I_{bdc}}{n_s}\left(\frac{V_{dc}}{2} - K_{pIdc}\left(I_{bdc}^* - I_{bdc}\right)\right)...\\ &+\frac{V_{ib\_err}}{2}\left(I_{bd} + I_{bq}\tan\left(\varphi_{ac}^*\right)\right)..\\ &+\frac{K_{pVs\_ac}}{2}\left(I_{bd} + I_{bq}\tan\left(\varphi_{ac}^*\right)\right)\left(V_S^* - V_S\right)\Bigg]\end{aligned} \tag{21}$$

$$\frac{dI_{bdc}}{dt} = \frac{K_{pIdc}}{n_s L_b}\left(I_{bdc}^* - I_{bdc}\right) \tag{22}$$

$$\frac{dI_{bd}}{dt} = \frac{K_{pId}}{n_s L_b}\left(I_{bd}^* - I_{bd}\right) - \frac{K_{pVs\_ac}}{L_b}\left(V_S^* - V_S\right) - \frac{V_{ib\_err}}{L_b} \tag{23}$$

$$\begin{aligned}\frac{dI_{bq}}{dt} = &\frac{K_{pIq}}{n_s L_b}\left(I_{bq}^* - I_{bq}\right) - \frac{K_{pVs\_ac}}{L_b}\tan\left(\varphi_{ac}^*\right)\left(V_S^* - V_S\right)\\ &-\frac{V_{ib\_err}}{L_b}\tan\left(\varphi_{ac}^*\right)\end{aligned} \tag{24}$$

$$\frac{dV_{ib\_err}}{dt} = K_{iVs\_ac}\left(V_S^* - V_S\right) \tag{25}$$

Several observations regarding the state equations may be made. First, d and q axis current cross-coupling has successfully been removed. Second, the capacitor voltage state equation (21) contains nonlinear terms that must be properly accommodated to ensure system stability. The steady-state operating conditions are determined by setting the derivative terms to zero:

$$I_{bd} = I_{bd}^* - \frac{n_s}{K_{pId}} V_{ib\_err} \tag{26}$$

$$I_{bq} = I_{bq}^* - \frac{n_s}{K_{pIq}} V_{ib\_err}\tan\left(\varphi_{ac}^*\right) \tag{27}$$

$$I_{bdc} = I_{bdc}^* \tag{28}$$

$$V_{ib\_err} = \frac{K_{pId}}{n_s}\left(I_{bd}^* - I_{bdc}^*\frac{V_{dc}}{V_{acd}}\right) \tag{29}$$

$$V_S = V_S^* \tag{30}$$

$$V_{dc} I_{bdc} = V_{ac} I_{bd}\,. \tag{31}$$

It may be observed that input and output power are balanced by (26-27), (29) and (31). More specifically, in the event of an improper current command by the converter controller, the local branch controllers are still able to compensate the current commands in order to achieve input

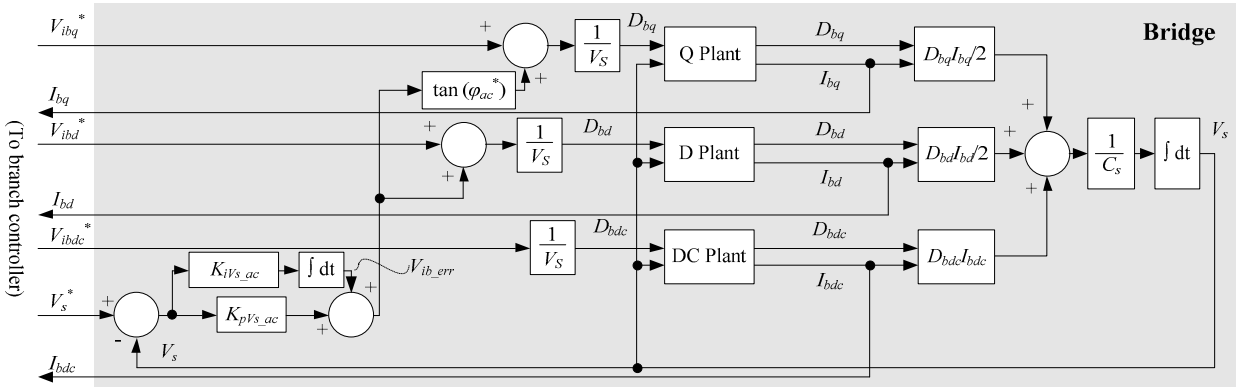

Fig. 9. Bridge controller block diagram including bridge plant and localized energy storage capacitor PI voltage regulator. I/O signals at left connect to the branch controller.

and output power balance, and thus regulate the energy storage capacitor voltage.

B. Small Signal Stability Analysis

In order to assess the dynamic properties of the controlled system, the state equations of (21-25) may be expressed in linearized state space form as

$$\dot{x} = Ax + Bu, \tag{32}$$

where x is the small signal state vector and u is the small signal input vector [8],

$$x = \begin{bmatrix} \delta I_{bd} & \delta I_{bq} & \delta I_{bdc} & \delta V_S & \delta V_{ib\_err} \end{bmatrix}^T \tag{33}$$

$$u = \begin{bmatrix} \delta V_{ac,d} & \delta V_{dc} & \delta I_{bd}^* & \delta I_{bq}^* & \delta I_{bdc}^* & \delta V_S^* \end{bmatrix}^T \tag{34}$$

and the matrices A and B represent the dynamic relationships between the small signal variables. The operating point of the system to study the small signal behavior is represented by

$$x_0 = \begin{bmatrix} I_{bd0} & I_{bq0} & I_{bdc0} & V_{S0} & V_{ib\_err0} \end{bmatrix}^T. \tag{35}$$

The stability of the operating point may be evaluated by examination of the eigenvalues for the system

$$\dot{x} = Ax, \tag{36}$$

where the small-signal state transition matrix, assuming unity power factor and steady-state conditions, is

$$A(x_0) = \begin{bmatrix} \frac{-K_{pId}}{n_s L_b} & 0 & 0 & \frac{K_{pVs}}{L_b} & \frac{-1}{L_b} \\ 0 & \frac{-K_{pIq}}{n_s L_b} & 0 & 0 & 0 \\ 0 & 0 & \frac{-K_{pIdc}}{n_s L_b} & 0 & 0 \\ \widetilde{A}_{41} & 0 & \widetilde{A}_{43} & \widetilde{A}_{44} & \widetilde{A}_{45} \\ 0 & 0 & 0 & -K_{iVs} & 0 \end{bmatrix} \tag{37}$$

and the remaining matrix elements are given as

$$\widetilde{A}_{41} = \frac{1}{V_{S0} C_S} \left[\frac{I_{bd0}}{n_s} K_{pId} + \frac{V_{ib\_err0}}{2} - \frac{K_{pVs\_ac} V_{S0}}{2} \right] \tag{38}$$

$$\widetilde{A}_{43} = \frac{1}{C_S V_{S0}} \left(\frac{2 K_{pIdc} I_{bdc0}}{n_s} \right) \tag{39}$$

$$\widetilde{A}_{44} = \frac{-1}{{V_{S0}}^2 C_S} \left[\frac{K_{pId} {I_{bd0}}^2}{2 n_s} + \frac{K_{pIdc} {I_{bdc0}}^2}{n_s} \cdots + \frac{V_{ib\_err0}}{2} I_{bd0} \right] \tag{40}$$

$$\widetilde{A}_{45} = \frac{I_{bd0}}{2 C_S V_{S0}}. \tag{41}$$

The eigenvalues of the linearized system can be examined to ensure the stability of the system with adequate margins in developing the controller design.

VI. Design Example

A converter design using the proposed controller structure was developed for 1 kW throughput and is suitable for use in residential grid-connected photovoltaic generation applications. Circuit parameters for the converter using reduced full bridge CSEBs are shown in TABLE I. . A choice of n_s = 5 results in a nominal 42V energy storage capacitor voltage, which with a 10% ΔV_S, permits the use of low-cost 60V automotive MOSFETs. The chosen modulation index M sets $n_s V_S$ = 207 V, which permits a 10% margin in duty ratio to ensure proper regulation in transient conditions. With series switch interleaving, the switching frequency is effectively multiplied by n_s, yielding an effective F_s of 500 kHz and resulting in a reasonable bridge inductance L_b. Furthermore, with such a high F_s the controller is immune to any and all switching behavior due to realistic current sensor bandwidth limitations, validating the use of averaged modeling techniques. Using the waveforms predicted by the averaged scalar model, appropriate capacitor and switch stresses can be computed and are included in TABLE I. .

Reasonable bandwidths of 1 kHz for d, q and dc current regulators are designed by examining the eigenvalues of (37). The gains for the voltage regulators are determined to realize the necessary bandwidth, set significantly less than 60 Hz, in light of the energy storage capacitor voltage carrying line frequency current components. The complete list of controller gains and their respective eigenvalues is shown in TABLE II.

TABLE I. Converter Design Parameters and Device Stresses

Parameter	Value	Parameter	Value
V_{dc}	48 V	M	0.9
I_{dc}	21 A	n_{br}	2
V_{ac1}, V_{ac2}	115 V_{rms}	F_s	100 kHz
cos(φ_{ac})	1	C_S	5000 µF
I_{ac1}, I_{ac2}	4.4 A_{rms}	L_b	30 µH
$I_{Cs,rms}$	5.2 A	$I_{D11,avg}$	5.2 A
$I_{Cs,peak}$	9.4 A	$I_{D22,avg}$	5.2 A
$I_{S12,avg}$, $I_{S21,avg}$	5.2 A	$I_{S12,rms}$, $I_{S21,rms}$	6.7 A

TABLE II. Controller Gains with Eigenvalues

Name	Value	Eigenvalue
K_{pId}, K_{pIq}, K_{pIdc}	0.9425	-1000 Hz (each)
K_{pVs_ac}	0.005	-1.6 Hz
K_{iVs_ac}	-0.00025	-0.0005 Hz

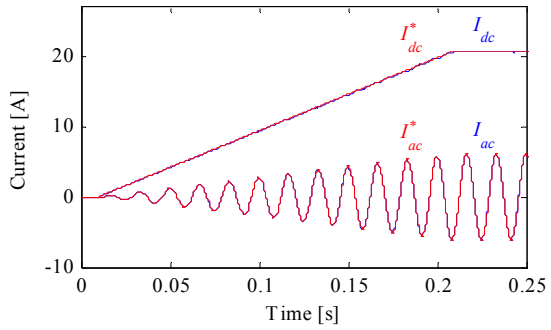

Fig. 10. Simulation results showing commanded and actual ac and dc terminal currents.

A. Simulation Results

The proposed 1 kW system was implemented in MATLAB/Simulink 2010a using PLECS 3.1 for averaged circuit model simulation. A 0-100% power ramp for 0.01-0.21s was simulated, resulting in the terminal currents shown in Fig. 10 with unity power factor. Terminal current command tracking is shown to be excellent, and a 80 mArms, 120 Hz harmonic in the dc current may be leveraged for effective maximum power point tracking (MPPT) [9]. Proper voltage regulator operation is also verified, achieving the commanded energy storage capacitor voltage within a reasonable time duration.

VII. Conclusions

The development of a dynamic phasor model in standard dq form suitable for developing classical control approaches has been outlined for a modular multilevel or bridge of bridge type of power converter. The controller uses decoupling between d and q circuit variables in the phasor domain to obtain excellent transient response. The control methodology has been discussed in detail with linear and nonlinear state space equations, steady-state behavior, and linearized state space representations provided. A power converter design example applied to a residential solar grid-tied inverter was shown and validated using computer simulations.

The d-q-dc phasor oriented model illustrated here can be extended to three phase BoB converters for ac-dc, dc-ac and ac-ac conversion and used for designing controllers for various applications such as motor drives, utility scale HVDC systems, etc. The model permits the use of classical control regulators in the design and assess the stability margins. The model may also be used to obtain linearized transfer functions for control variables so that frequency response functions can be evaluated and used in the design process.

Appendix

Variable	Description
C_S	Energy storage capacitor
d_b	Bridge duty ratio
I_{ac}	Terminal ac current
i_b	Bridge current
I_{dc}	Terminal dc current
I_{ground}	Terminal ground current (ac & dc)
L_b	Bridge inductance
M	Modulation index
n_s	Number of series-connected bridges per branch
V_{ac}	Terminal ac voltage
v_{iB}	Internal bridge voltage
V_{dc}	Terminal dc voltage
V_{ib_err}	Capacitor voltage regulator integral state
V_S	Bridge capacitor voltage

Acknowledgment

The authors wish to acknowledge the support provided by the Wisconsin Electric Machines and Power Electronics Consortium (WEMPEC) of the University of Wisconsin–Madison.

References

[1] D. C. Ludois, J. K. Reed, and G. Venkataramanan, "Hierarchical control of bridge-of-bridge multilevel power converters," *IEEE Transactions on Industrial Electronics,* vol. 57, pp. 2679-2690, 2010.

[2] A. Lesnicar and R. Marquardt, "A new modular voltage source inverter topology," in *Proc. European Conference on Power Electronics (EPE)*, 2003.

[3] G. P. Adam, O. Anaya-Lara, and G. Burt, "Multi-terminal dc transmission system based on modular multilevel converter," in *Proc. 44th International Universities Power Engineering Conference (UPEC)*, Glasgow, UK, 2009.

[4] Y. Huang, F. Z. Peng, J. Wang, and D.-w. Yoo, "Survey of the Power Conditioning System for PV Power Generation," in *Power Electronics Specialists Conference, 2006. PESC '06. 37th IEEE*, 2006, pp. 1-6.

[5] S. B. Kjaer, J. K. Pedersen, and F. Blaabjerg, "A review of single-phase grid-connected inverters for photovoltaic modules," *IEEE Transactions on Industry Applications,* vol. 41, pp. 1292-306, 2005.

[6] J. Wiles, *Photovoltaic Power Systems and the 2005 National Electrical Code: Suggested Practices*, Electronic Version 1.91 ed. Albuquerque: Sandia National Laboratory, 2010.

[7] D. W. Novotny and T. A. Lipo, *Vector control and dynamics of AC drives*. New York: Oxford University Press, 1996.

[8] R. C. Dorf and R. H. Bishop, *Modern control systems*, 9th ed. Upper Saddle River, NJ: Prentice Hall, 2001.

[9] A. Cocconi, S. Cuk, and R. D. Middlebrook, "High-Frequency Isolated 4kW Photovoltaic Inverter for Utility Interface," *Powerconversion International,* vol. 10, p. 16p, 1984.